JOURNAL OF COMPUTATIONAL PHYSICS 112, 298–307 (1994)

A Finite-Difference Algorithm for Multiple Moving Boundary Problems Using Real and Virtual Grid Networks

MOHAMED ZERROUKAT AND CHRIS R. CHATWIN

Department of Mechanical Engineering, University of Glasgow, Glasgow G12 8QQ, Scotland, United Kingdom

Received February 22, 1993

Most numerical methods developed for moving boundary or Stefan problems deal with the case of a single moving boundary (MB) separating two different media. Although this is applicable to a large number of engineering problems, there are many problems where more than one MB exists simultaneously during the process. A heat transfer process involving heating of a solid, melting, and partial vaporisation of liquid can be considered as a three-phase Stefan or two MB problem, where the time of appearance and disappearance of phases are to be determined as a part of the solution. An explicit unconditionally stable numerical scheme for such problems is presented and tested herein. The approach originates from the explicit variable time step (EVTS) method, developed by the same authors, for single MB problems. During the vaporisation stage, where two MBs exist simultaneously, the method uses a virtual distorted grid network moving in parallel to the vapour/liquid interface in order to determine its position vis-à-vis the real grid network. The method has been tested by solving both the collapse of an adiabatic wall and a normalised two-MB problem whose exact solution is known.

1. INTRODUCTION

Many physical processes are modelled as moving boundary problems (MBPs), in which partial differential equations are utilised for adjacent domains separated by boundaries whose movement must be determined as an integral part of the solution. The singularities at the moving boundaries add complexity as frequently different properties are required to describe the phenomena in each distinct region. Due to their wide range of applications, efficient analytical or numerical solutions of MBPs are still of considerable interest to the scientific and engineering community. Since the conditions at the fixed and moving boundaries are often complex, the analytical solution is generally impossible to obtain. Therefore, recourse is often made to numerical methods where most boundary conditions can be accommodated.

Heat conduction problems with phase transformations are classified as MBPs but usually referred to as Stefan problems according to J. Stefan [1] who published the first paper dealing with this subject. Most numerical methods for moving boundary problems are generally conceived for one MB separating two phases [2]. Whilst single MB problems are of considerable utility in modelling a whole class of engineering problems, many engineering and physical problems must be modelled with two or more MBs. Heat conduction problems with heating of solid, melting, and partial vaporisation of liquid is one such problem.

Bonnerot and Jamet [3] have introduced a conservative finite element method which can be used to solve such problems. They applied a modified and extended form of their third-order-accuracy discontinuous finite element method [4]. It adopts a curved triangular element for each appearing or disappearing phase, whilst a curved trapezoidal element is employed elsewhere (this method will be referred to as the BJ method). However, finite element techniques are time consuming and less amenable to vectorisation than finite difference methods.

In this paper an alternative faster and simpler method, based on finite differences, is presented. The explicit variable time step (EVTS) method [5] is extended to deal with multi-phase Stefan problems. The present scheme adopts a fixed time-space grid network during the pre-melting stage, a variable time step grid network during the melting and vaporisation stages, and uses explicit finite difference replacements for the partial and ordinary differential equations. During the vaporisation period, which is the most difficult period to compute, the method uses the approach of fixing the liquid solid (L/S) interface at a real space grid line and determines the time step iteratively. Having arranged the solution scheme, so that the L/S interface always coincides with a spatial grid line. A further problem is to determine the corresponding position of the vapour/liquid (V/L) interface. Therefore the method uses a virtual distorted grid network moving in parallel to the second MB; this permits the explicit determination of the position of the second MB as well as the temperature throughout the liquid region between the two moving boundaries.

0021-9991/94 $6.00

As in EVTS, the virtual sub-interval elimination technique (VSIET) [5] is incorporated throughout all the different stages of the computation—to ensure that stability is automatically maintained irrespective of the mesh size. As a result of incorporating the VSIET the accuracy of the present method is unaffected by the velocity of the MBs.

The numerical method is presented for a general heat transfer problem which will be described in Section 2. For validation, the method was used to solve the collapse of a solid wall due to a heat flux input at one boundary with an adiabatic condition at the other [3]. The problem involves heating of the solid, melting, vaporisation, and finally complete collapse of the wall when the solid phase disappears. Numerical results are compared with those of the BJ finite element method and show good agreement. Furthermore, a normalised two-MB problem—which has an exact analytical solution—was considered and numerical results show that the method achieves good accuracy relative to the exact solution which is used as a reference standard.

2. DESCRIPTION OF MULTIPHASE STEFAN PROBLEM

Consider a solid material of infinite transverse dimensions and thickness a to be subjected to a variable source of heat $F(t)$ at one extremity ($x=0$) and in contact with a fluid at a constant temperature T_0 at the other ($x=a$). Assuming that the heat transfer is one-dimensional and that the material thermal properties are constant within each phase but differ from one phase to another; depending on the process duration, the following stages will occur.

2.1. *Heating of the Solid Stage* ($0 \leqslant t \leqslant t_m$; Fig. 1a)

Due to the positive heat flux input, the temperature throughout the solid increases with no change of phase. The governing equations for this stage are

$$C_s \frac{\partial T_s}{\partial t} = K_s \frac{\partial^2 T_s}{\partial x^2}, \qquad M(t) \leqslant x \leqslant a, \qquad 0 \leqslant t \leqslant t_e, \quad (1)$$

$$-K_s \left(\frac{\partial T_s}{\partial x}\right) = F(t), \qquad x=0, \qquad 0 \leqslant t \leqslant t_m, \quad (2)$$

$$-K_s \left(\frac{\partial T_s}{\partial x}\right) = h(T_s(x,t) - T_0), \qquad x=a, \qquad 0 \leqslant t \leqslant t_e, \quad (3)$$

where $T(x, t)$ is the temperature at depth x time t; C, K, $\alpha = K/C$, and h are heat capacity per unit volume, thermal conductivity, diffusivity, and convective heat transfer coefficient, respectively. $M(t)$, t_m, and t_e denote the liquid/solid interface position, the time at which melting starts, and the time at which the heat transfer process ends, respectively.

2.2. *Melting Stage* ($t_m \leqslant t \leqslant t_v$; Fig. 1b)

When the surface temperature $T(0, t)$ reaches the melting point of the material (T_m) a MB, $x = M(t)$, appears which separates the liquid from the solid. It is assumed that the liquid and the solid have the same density and consequently there is no displacement of the liquid surface; therefore, the liquid occupies the region $0 \leqslant x \leqslant M(t)$ and the solid occupies the region $M(t) \leqslant x \leqslant a$. The liquid/solid interface $M(t)$ moves in the x direction and temperature increases throughout the solid and liquid regions. In addition to (1) and (3), the equations

$$C_l \frac{\partial T_l}{\partial t} = K_l \frac{\partial^2 T_l}{\partial x^2}, \qquad V(t) \leqslant x \leqslant M(t), \qquad t_m \leqslant t \leqslant t_e, \quad (4)$$

$$-K_l \left(\frac{\partial T_l}{\partial x}\right) = F(t), \qquad x=0, \qquad t_m \leqslant t \leqslant t_v, \quad (5)$$

$$\lambda_m \frac{dM}{dt} = K_s \left(\frac{\partial T_s}{\partial x}\right) - K_l \left(\frac{\partial T_l}{\partial x}\right), \qquad x = M(t), \qquad t_m \leqslant t \leqslant t_e, \quad (6)$$

are necessary to describe this stage, where λ_m, $V(t)$, and t_v are latent heat of fusion per unit volume, the vapour/liquid interface position, and the time at which vaporisation starts, respectively. The subscripts l and s distinguish liquid and solid phases, respectively.

2.3. *Vaporisation Stage* ($t_v \leqslant t \leqslant t_e$; Fig. 1c)

When the surface temperature $T(0, t)$ reaches the vaporisation point (T_v) of the material, a second MB, $x = V(t)$, appears which separates the liquid from the vapour. Assuming that the vapour is removed as soon as it appears (i.e., only two phases remain), the liquid occupies

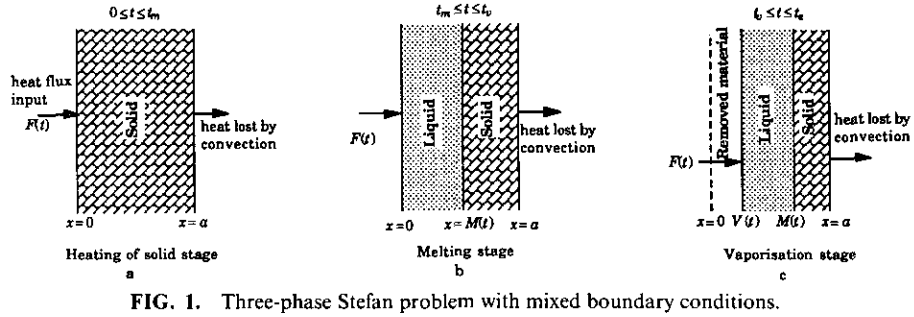

FIG. 1. Three-phase Stefan problem with mixed boundary conditions.

the region $V(t) \leqslant x \leqslant M(t)$ and the solid occupies $M(t) \leqslant x \leqslant a$ (the ablation case, where the whole liquid region is instantaneously evaporated, is not considered in this work). The two MBs continue to propagate in the x direction and the temperature increases throughout the solid and liquid regions until the time at which the heat transfer process ends (t_e). The final time for the test problems in Section 4 is the time for complete melting (i.e., when the liquid/solid interface $M(t)$ has reached $x = a$). This stage is governed by (1), (3), (4), (6) and the following condition at the second MB, $x = V(t)$,

$$\lambda_v \frac{dV}{dt} = K_l \left(\frac{\partial T_l}{\partial x}\right) + F(t), \qquad x = V(t), \qquad t_v \leqslant t \leqslant t_e, \tag{7}$$

where λ_v is the latent heat of vaporisation per unit volume.

The following conditions apply for all three stages:

$$\begin{aligned} V(t) &= 0, && t \leqslant t_v \\ M(t) &= 0, && t \leqslant t_m \\ T(x, t) &= T_m, && x = M(t), \quad t \geqslant t_m, \\ T(x, t) &= T_v, && x = V(t), \quad t \geqslant t_v, \\ T(x, 0) &= T_0, && \forall x \in [0, a]. \end{aligned} \tag{8}$$

3. NUMERICAL COMPUTATION SCHEME

In this section, a description of the numerical scheme for the problem described in Section 2 is given in order of the computational sequences, assuming that all the stages occurred during the process. As previously mentioned, the numerical method adopts a fixed time-space grid network during the heating of solid stage and a variable time step grid network in the melting and vaporisation stages. The total thickness a is divided into a fixed number of space intervals N, of length Δx, during the whole computation process.

Let j_m and j_v be the time step indices so that $t_{j_m} \leqslant t_m \leqslant t_{j_m+1}$ and $t_{j_v} \leqslant t_v \leqslant t_{j_v+1}$. The notation $T_{i,j}$ stipulates the value of T at the real grid point in the $(x-t)$ domain given by the co-ordinates

$$\left(x_i = i\,\Delta x,\ t_j = \begin{cases} j\,\Delta t_0, & j < j_m \\ t_m + \sum_{q=j_m}^{j-1} \Delta t_q, & j \geqslant j_m \end{cases} \right), \tag{9}$$

and V_j is the value of V at the time t_j.

3.1. *Heating of Solid Stage*

In this stage, where there are no phase changes, a fixed time step Δt_0 is chosen arbitrarily. The notation $\bar{\psi}_{i,j,n,p}$ is used to indicate the value of the variable ψ at the virtual grid point in the $(x-t)$ domain given by the co-ordinates

$$\left(x_i = i\,\Delta x,\ t_{j,n,p} = \left(j + \frac{n}{p}\right) \Delta t_0 \right) \tag{10}$$

and the notation (j, n, p) represents the virtual sub-step (VSS) at the time $t_{j,n,p}$, where n is the VSS index.

The temperature distribution at each VSS (j, n, p_0), where $\{1 \leqslant j \leqslant j_m, 1 \leqslant n \leqslant p_0\}$, is calculated from that of the previous VSS $(j, n-1, p_0)$, using

$$\bar{T}_{i,j,n,p_0} = \bar{T}_{i,j,n-1,p_0} \exp\left(-\frac{r_c}{\bar{T}_{i,j,n-1,p_0}} \bar{\psi}_{i,j,n-1,p_0} \right), \qquad i = 0, N, \tag{11}$$

where

$$\bar{\psi}_{i,j,n,p} = \begin{cases} 2\left(\bar{T}_{i,j,n,p} - \bar{T}_{i+1,j,n,p} - \left(\frac{\Delta x}{K_s}\right) \hat{F}_{j,n,p} \right), \\ \qquad i = 0, \\ (2\bar{T}_{i,j,n,p} - \bar{T}_{i-1,j,n,p} - \bar{T}_{i+1,j,n,p}), \\ \qquad 1 \leqslant i \leqslant N-1, \\ 2\left(\left(1 + \frac{h\,\Delta x}{K_s}\right) \bar{T}_{i,j,n,p} - \bar{T}_{i-1,j,n,p} \right. \\ \qquad \left. - \left(\frac{h\,\Delta x}{K_s}\right) T_0 \right), \qquad i = N, \end{cases} \tag{12}$$

where

$$\hat{F}_{j,n,p} = \tfrac{1}{2}\{F(t_{j,n,p}) + F(t_{j,n+1,p})\} \tag{13}$$

$$p_0 = \text{int}\left(\frac{\alpha_s}{r_f} \frac{\Delta t_0}{\Delta x^2}\right) + 1, \qquad r_c = \frac{\alpha_s}{p_0} \frac{\Delta t_0}{\Delta x^2}, \tag{14}$$

where "int(y)" defines the smallest integer less than y; r_f is an arbitrary fixed value of Fourier number ($r_f \leqslant \frac{1}{2}$).

The temperature distribution at the last VSS $(j, n = p_0, p_0)$ of each time step is assigned to the real grid; the temperature distribution at the time $t = t_{j+1}$ is given by

$$T_{i,j+1} = \bar{T}_{i,j,p_0,p_0}, \qquad i = 0, N. \tag{15}$$

In order to avoid stability problems when the rate of the heat flux input prescribed at $x = 0$ is relatively high, it is necessary to calculate the temperature distribution at the first time step $j = 1$ analytically (see Appendix).

Suppose at some intermediate VSS (j_m, n_m, p_0), the surface temperature exceeds the melting point T_m, then the time at which the melting starts (t_m) is given by

$$t_m = j_m\,\Delta t_0 + (n_m - 1)\left(\frac{\Delta t_0}{p_0}\right) + \left(\frac{-\Delta x^2}{\alpha_s \bar{\psi}_{0,j_m,n_m-1,p_0}}\right) \times \text{Log}_e\left(\frac{T_m}{\bar{T}_{0,j_m,n_m-1,p_0}}\right). \tag{16}$$

3.2. *Melting Stage*

For Sections 3.2 and 3.3 we use the notation $\bar{\psi}^{k}_{i,j,n,p}$ to indicate the kth iterated value of the variable ψ at the virtual grid point in the $(x-t)$ domain given by the co-ordinates

$$\left(x_i = i\,\Delta x,\ t^{k}_{j,n,p} = t_m + \sum_{q=j_m}^{j-1} \Delta t_q + n\,\frac{\Delta t^{k}_{j}}{p^{k}_{j}}\right), \tag{17}$$

where Δt_q is the time necessary for the moving boundary $M(t)$ to move from the position $x = x_{q-j_m}$ to $x = x_{q+1-j_m}$.

For this stage, the temperature throughout the liquid and solid regions as well as the position of the moving boundary $M(t)$ are computed using the EVTS method [5]. At some VSS (j_v, n_v, p), the surface temperature will exceed the vaporisation temperature (T_v); once this occurs the vaporisation time (t_v) is calculated using

$$t^{k}_{v} = t_m + \sum_{q=j_m}^{j_v-1} \Delta t_q + \left(\frac{n^{k}_{v}-1}{p^{k}_{j_v}}\right)\Delta t^{k}_{j_v} + \left(\frac{-\Delta x^2}{\alpha_l \bar{\psi}^{k}_{0,j_v,n_v-1,p}}\right) \times \mathrm{Log_e}\left(\frac{T_v}{\bar{T}^{k}_{0,j_v,n_v-1,p}}\right). \tag{18}$$

After determination of the time at which the vaporisation starts, computation is carried out similarly to melting until the condition given by (31) is verified. Consequently a liquid region of thickness $x = x_1$ near the surface will be superheated (i.e., temperature is above the vaporisation point).

3.3. *Vaporisation Stage*

At the beginning of computation of this stage, the liquid region of thickness $x = x_1$ is superheated, equilibrium is established by vaporisation of the superheated liquid to a liquid depth of $x = x_2$. A mathematical expression similar to that suggested by Heitz and Westwater [6] and later developed by Hsu *et al.* [7] for a superheated solid is used:

$$x_2 = \frac{C_l}{\lambda_v}\int_0^{x_1} (T_l(x, t_{j_v+1}) - T_v)\,dx. \tag{19}$$

Generally the superheated region extends less than one space increment; therefore $T_l(x, t_{j_v+1})$ can be approximated by a polynomial of degree one in the region $0 \leqslant x \leqslant x_1$. Hence, the depth of the initially vaporised material is determined directly without recourse to numerical integration.

At any time during the vaporisation stage, where two MBs exist simultaneously, both the energy balance conditions given by (6) and (7) must be satisfied at each time step. The method ensures that $M(t)$ moves a space increment Δx and determines iteratively the time step Δt necessary for that move. During each VSS at each iteration, the position of $V(t)$ is adjusted to satisfy the condition given by (7); hence, the problem is simplified, as in Section 2.2, where the test for halting the iterations is carried out at the liquid/solid interface only. In order to achieve this, it is assumed that there is a virtual distorted grid network $(y-t)$ formed by $V(t)$, and two lines (one at Δx and the other at $2\,\Delta x$ relative to $V(t)$) moving in parallel with $V(t)$ (see Fig. 2b). To trans-

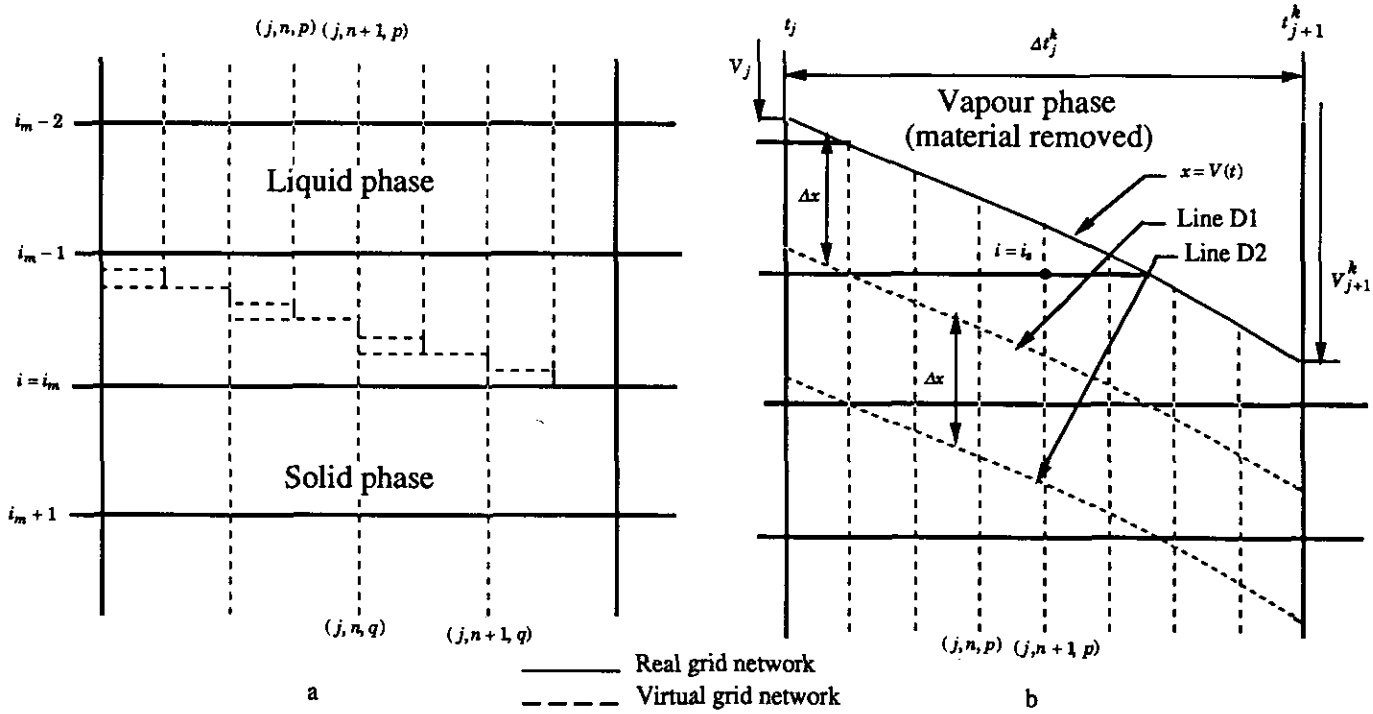

FIG. 2. Discretisation around the moving boundaries together with both real and virtial grid networks: (a) around the liquid/solid interface, $x = M(t)$; (b) around the vapour/liquid interface, $x = V(t)$.

form the equations from the original grid $(x-t)$ to $(y-t)$ the transformation $y=x+V(t)$ was used, applying the chain rule, Eq. (4) becomes

$$\frac{\partial T_l}{\partial t}=\frac{K_l}{c_l}\frac{\partial^2 T_l}{\partial y^2}-\frac{dV}{dt}\frac{\partial T_l}{\partial y}. \tag{20}$$

Writing Eq. (20) between two VSSs, (j, n, p) and $(j, n+1, p)$, and assuming a linear propagation of $V(t)$ between each two VSSs, (dV/dt) can be approximated by $\bar{\chi}_{j,n,p}$ which represents the variation of $V(t)$ during the course of (j, n, p) and $(j, n+1, p)$, Eq. (20) becomes

$$\frac{\partial \bar{T}_l}{\partial t}=\alpha_l\frac{\partial^2 \bar{T}_l}{\partial y^2}-\bar{\chi}_{j,n,p}\frac{\partial \bar{T}_l}{\partial y}. \tag{21}$$

Following the procedure of Bhattacharya [8, 9], Eq. (21) has a difference solution of the form of (11). The temperature $\bar{\theta}^k_{j,n+1,p}$—at the first virtual distorted grid line D1, which is situated Δx from the position of the MB $x=V(t)$, at $(j, n+1, p)$—is given by

$$\bar{\theta}^k_{j,n+1,p}=\bar{\theta}^k_{j,n,p}\exp(-r^k_{cl,j}\bar{\phi}^k_{j,n,p}), \tag{22}$$

where

$$\begin{aligned}\bar{\phi}^k_{j,n,p}=&\left(\frac{\Delta x\,\bar{\chi}^k_{j,n,p}}{2\alpha_l}\right)^2+\left(\frac{1}{\bar{\theta}^k_{j,n,p}}\right)\Bigg\{(2\bar{\theta}^k_{j,n,p}-\bar{\varphi}^k_{j,n,p}-T_v)\\&-\left(\frac{\Delta x\,\bar{\chi}^k_{j,n,p}}{2\alpha_l}\right)(T_v-\bar{\varphi}^k_{j,n,p})\\&-\left(\frac{\Delta x\,\bar{\chi}^k_{j,n,p}}{2\sqrt{2}\,\alpha_l}\right)^2(T_v+\bar{\varphi}^k_{j,n,p})\Bigg\},\end{aligned} \tag{23}$$

where p^k_j and $r^k_{cl,j}$ are defined as

$$p^k_j=\operatorname{int}\left(\frac{\alpha_l}{r_f}\frac{\Delta t^k_j}{\Delta x^2}\right)+1,\qquad r^k_{cl,j}=\frac{\alpha_l}{p^k_j}\frac{\Delta t^k_j}{\Delta x^2}. \tag{24}$$

As the position of $V(t)$ is conditioned to satisfy the energy balance at $x=V(t)$, replacing (7) by a finite difference gives

$$\bar{\chi}^k_{j,n,p}=\left(\frac{\Delta t^k_j}{\lambda_v p^k_j}\right)\left\{\hat{F}_{j,n,p}-\frac{K_l}{\Delta x}(T_v-\bar{\theta}^k_{j,n+1,p})\right\}. \tag{25}$$

Since $\bar{\chi}^k_{j,n,p}$ is not known, to solve (22), (23), and (25), an iterative procedure is used starting with $\bar{\chi}^{k,0}_{j,n,p}=\bar{\chi}^k_{j,n-1,p}$. Due to the small length of sub-intervals, $\bar{\chi}^k_{j,n,p}$ is generally determined in two iterations only.

After determination of $\bar{\chi}^k_{j,n,p}$, the temperature at the surface node, $i=i_s$—which is the first node below $x=V(t)$ in the original (non-distorted) grid (see Fig. 2b), at the VSS $(j, n+1, p)$—can be interpolated by using simple interpolation from the temperature at the virtual distorted line D1 and the temperature at the moving boundary $x=V(t)$,

$$\begin{aligned}\bar{T}^k_{i_s,j,n+1,p}=&\bar{\theta}^k_{j,n+1,p}\left[1-\operatorname{mod}\left(\frac{\bar{V}^k_{j,n+1,p}}{\Delta x},1\right)\right]\\&+T_v\left[\operatorname{mod}\left(\frac{\bar{V}^k_{j,n+1,p}}{\Delta x},1\right)\right],\end{aligned} \tag{26}$$

where $\operatorname{mod}(y, x)=y-x\,\operatorname{int}(y/x)$ and $\bar{V}^k_{j,n+1,p}$ is given by

$$\bar{V}^k_{j,n+1,p}=V_{j-1}+\sum_{n=0}^{n}\bar{\chi}^k_{j,n,p}. \tag{27}$$

Now the computation of temperatures at the virtual grid points, $i>i_s$, throughout the liquid are carried out in a manner similar to that in Section 2.2. It can be seen from (23) that for the next VSS, the temperature $\bar{\varphi}^k_{j,n+1,p}$—at the second virtual distorted line D2, at $(j, n+1, p)$—must be known. In order to minimise the CPU time, it is calculated by a simple interpolation from temperatures at the original (non-distorted) grid and it is given by

$$\begin{aligned}\bar{\varphi}^k_{j,n+1,p}=&\bar{T}^k_{i_s+2,j,n+1,p}\left[1-\operatorname{mod}\left(\frac{\bar{V}^k_{j,n+1,p}}{\Delta x},1\right)\right]\\&+\bar{T}^k_{i_s+1,j,n+1,p}\left[\operatorname{mod}\left(\frac{\bar{V}^k_{j,n+1,p}}{\Delta x},1\right)\right].\end{aligned} \tag{28}$$

The position of $V(t)$ and the temperature distribution throughout the liquid and solid regions (computation of temperature distribution throughout the solid region is similar to Section 2.2) at the time $t=t^k_{j+1}$ are given by

$$V^k_{j+1}=V_j+\sum_{n=0}^{p^k_j-1}\bar{\chi}^k_{j,n,p} \tag{29}$$

$$T^k_{i,j+1}=\begin{cases}\bar{T}^k_{i,j,p^k_j,p}, & i=i_s, i_m-1,\\ T_m, & i=i_m,\\ \bar{T}^k_{i,j,q^k_j,q}, & i=i_m+1, N.\end{cases} \tag{30}$$

Once the temperature distribution throughout the solid and liquid regions at the time $t=t^k_{j+1}$ has been estimated from (30), all the intermediate time steps are virtual and are progressively eliminated; the criterion used for convergence of the temperature field is

$$|\varepsilon^k_j|\leqslant\varepsilon_{\min}, \tag{31}$$

where $\varepsilon_{\min}$ is the time step error allowed to stop iterations and ε^k_j is given by

$$\varepsilon^k_j=100\times\frac{\Delta t^k_j-\xi^k_j}{\Delta t^k_j}, \tag{32}$$

where

$$\xi_j^k = \left\{ \left(\frac{1}{\lambda_m \Delta x^2} \right) [K_l(T^k_{i_m-1,j+1} - T_m) - K_s(T_m - T^k_{i_m+1,j+1})] \right\}^{-1}. \quad (33)$$

If Eq. (31) is not satisfied, a relaxation procedure is applied to determine the time step for the $(k+1)$th iteration,

$$\Delta t_j^{k+1} = \Delta t_j^k \left(1 - \frac{\varepsilon_j^k}{100\omega} \right), \quad (34)$$

where ω is a relaxation factor and $\Delta t_j^0 = \Delta t_{j-1}$.

Remark 1. When the energy balance at $x = M(t)$ takes into account the temperature gradient in one phase only as in test problem 2 of Section 4, the time step at the next iteration Δt_j^{k+1} can be determined by a similar procedure to that suggested by Gupta and Kumar [10] (i.e., $\Delta t_j^{k+1} = \xi_j^k$). For the case of two MBs such as problem 2, the procedure may converge in certain cases and may not in others; however, Eq. (33) has shown satisfactory convergence for all the computations performed.

4. TEST PROBLEMS

PROBLEM 1 (Collapse of a solid wall). The method described in Section 3 has been used to solve the collapse of a solid wall due to a constant heat flux input F at $x = 0$, whilst the other extremity $x = a$ is thermally insulated (i.e., $\partial T/\partial x = 0$ at $x = a$) [3]. Solving this problem is similar to solving the problem previously described in Section 2 but with a convective heat transfer coefficient $h = 0$. Bonnerot and Jamet [3] demonstrated the solution of the problem with two different sets of data.

PROBLEM 1a.

$$\begin{aligned} &a = 1, \quad T(x,0) = 27, \quad F = 2500, \\ &C_l = C_s = 4.944, \quad K_l = K_s = 0.259, \\ &\lambda_m = 2160, \quad \lambda_v = 37200, \\ &T_m = 1454, \quad T_v = 3000. \end{aligned} \quad (35)$$

This data set permits all three stages (i.e., heating of solid, melting, and vaporisation) to occur. For the present method a choice of $\Delta x = 0.02$ was used so as to have approximately the same total number of grid points as the BJ method, where $\Delta t/\Delta x = \frac{1}{16}$. For the present method, which will be referred to as the ZC method, a relaxation factor $\omega = 3.0$, $\varepsilon_{\min} = 0.05\%$, and $r_f = 0.30$ have been used. A comparison of results using the BJ and ZC methods is given in Table I and Figs. 1, 2, and 3; these are discussed in Section 5.

TABLE I

Problem 1a: Comparison of t_m, t_v, t_e, and $V(t_e)$ for Different Time increments Δt

Δt	t_m	t_v	t_e	$V(t_e)$
BJ method [3]				
1/4	0.36150	1.63034	9.75464	0.28351
1/8	0.32897	1.63611	9.40210	0.26703
1/16	0.32767	1.63446	9.38719	0.26633
1/32	0.32768	1.63439	9.38708	0.26632
ZC method				
1/4	0.32740	1.58887	9.15907	0.26318
1/8	0.32660	1.58783	9.15828	0.26319
1/16	0.32580	1.58705	9.15745	0.26318
1/32	0.32494	1.58620	9.15670	0.26319

Remark 2. Since the time step during the melting and vaporisation stages for the ZC method is variable, the Δt quoted in Tables I and II is the Δt_0 defined in Section 3.1.

PROBLEM 1b.

$$\begin{aligned} &a = 1, \quad T(x,0) = 27, \quad F = 2500, \\ &c_l = c_s = 1.041\rho, \quad K_l = 1.73, \quad K_s = 0.865, \\ &\lambda_m = 400\rho, \quad \lambda_v = 10700\rho, \\ &T_m = 638, \quad T_v = 2480, \quad \rho = 2.77. \end{aligned} \quad (36)$$

where ρ is the material density.

With this data set, the melting interface reaches the adiabatic boundary before vaporisation occurs; the process is therefore reduced to a single MB problem. The same parameters (ZC $\{\Delta x, r_f, \omega, \varepsilon_{\min}\}$; BJ $\{\Delta t/\Delta x, \varepsilon\}$) have been

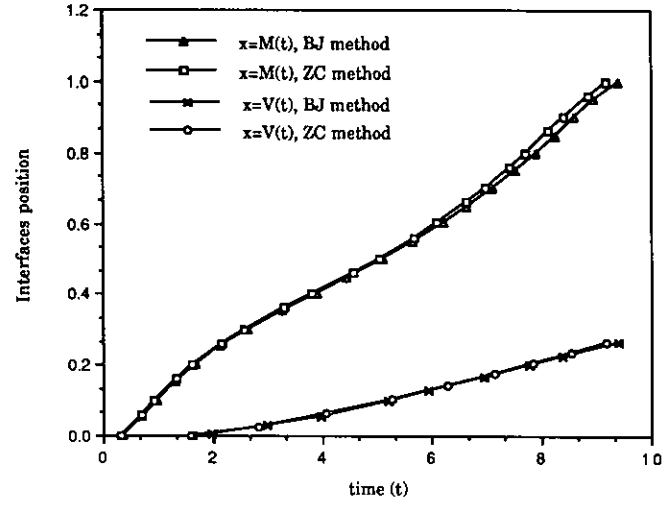

FIG. 3 (Problem 1a). Position of the liquid/solid and vapour/liquid interfaces versus time.

TABLE II

Problem 1b: Comparison of t_m, t_e, and $T(0, t_e)$ for Different Time Increments Δt

Δt	t_m	t_e	$T(0, t_e)$
BJ method [3]			
1/4	0.23485	1.92536	2349.18
1/8	0.23401	1.92383	2347.98
1/16	0.23400	1.92381	2347.96
ZC method			
1/4	0.23352	1.89063	2341.45
1/8	0.23398	1.88747	2341.40
1/16	0.23390	1.88719	2341.40

used as in Problem 1a. The comparison of results of the ZC and BJ methods is shown in Table II and Figs. 4, 5, and 6; these are discussed in Section 5.

PROBLEM 2. In order to further validate the accuracy of the method, the following normalised two-MB problem, whose exact analytical solution is known, was considered. A solid material melts due to a variable heat flux input applied at the liquid surface, the temperature throughout the solid region is always assumed to remain at the melting point. The governing equations are

$$\frac{\partial T_l}{\partial t} = \alpha_l \frac{\partial^2 T_l}{\partial x^2}, \qquad V(t) \leqslant x \leqslant M(t), \qquad 0 \leqslant t \leqslant t_e, \tag{37}$$

$$\frac{\partial T_l}{\partial x} = -\exp(\alpha_l t), \qquad x = 0, \qquad 0 \leqslant t \leqslant t_v, \tag{38}$$

$$\frac{1}{\alpha_l}\frac{dM}{dt} = -\frac{\partial T_l}{\partial x}, \qquad x = M(t), \qquad 0 \leqslant t \leqslant t_e, \tag{39}$$

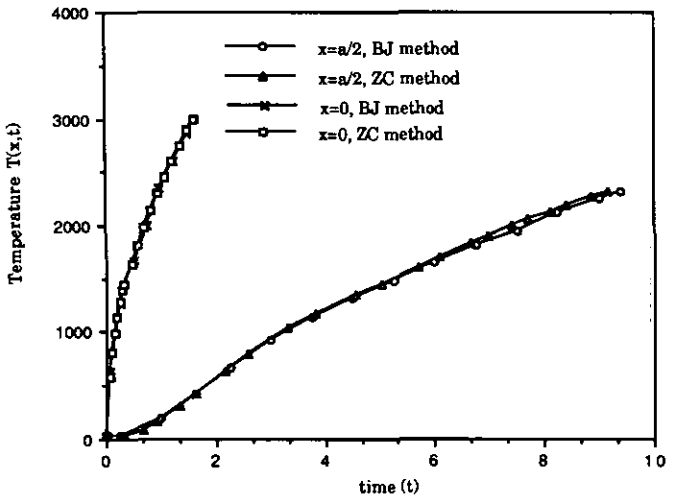

FIG. 4 (Problem 1a). Temperature versus time at different depths.

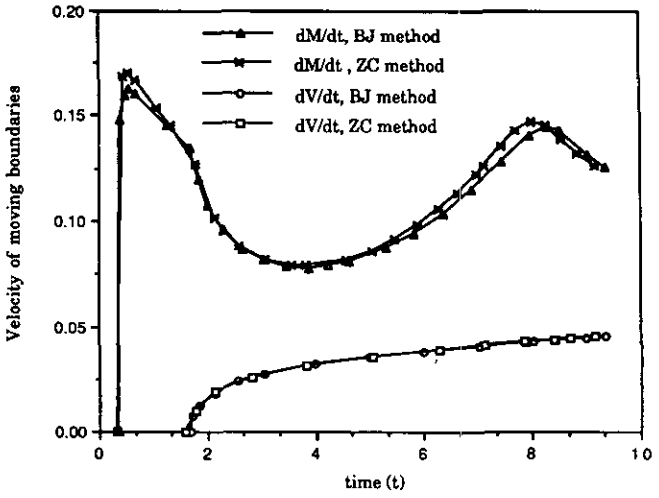

FIG. 5 (Problem 1a). Velocity of the moving boundaries versus time.

$$\frac{T_v}{\alpha_l}\frac{dV}{dt} = \exp(\alpha_l t_v), \qquad t_v \leqslant t \leqslant t_e, \tag{40}$$

$$T_l(x, t) = \begin{cases} T_m = 1.0, & M(t) \leqslant x \leqslant 1.0, \quad t \geqslant 0, \\ T_v, & x = V(t), \quad t \geqslant t_v, \end{cases} \tag{41}$$

$$M(0) = 0, \qquad T_l(x, 0) = 1.0 \qquad \text{for} \quad 0 \leqslant x \leqslant 1.0. \tag{42}$$

The exact analytical solution is given by

$$T_l(x, t) = \exp(\alpha_l t - x), \qquad M(t) = \alpha_l t, \qquad V(t) = \alpha_l (t - t_v)$$
$$t_v = \frac{1}{\alpha_l}\operatorname{Log}_e(T_v), \qquad t_e = \frac{1}{a_l}. \tag{43}$$

Since in this particular problem the condition at the second moving boundary (vapour/liquid) is not coupled to the temperature gradient in the liquid region; the virtual dis-

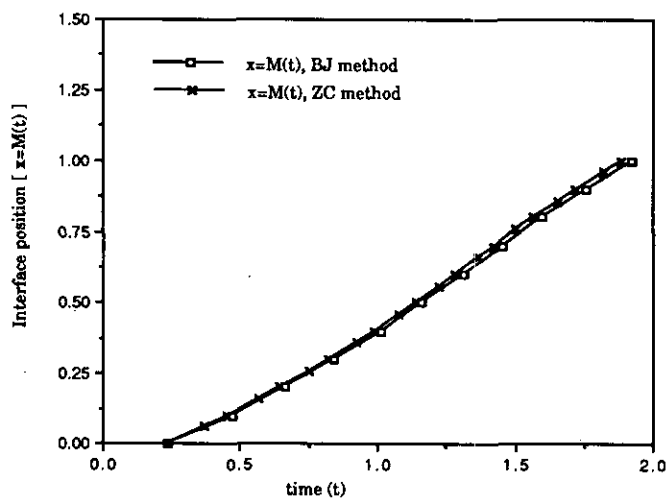

FIG. 6 (Problem 1b). Position of the liquid/solid interface versus time.

TABLE III

Problem 2: A Comparison of Computed History of the Moving Boundaries $M(t)$ and $V(t)$ with the Analytical Solution

$M(t)$	t_{Nu}	t_{An}	PDt	V_{Nu}	V_{An}	PDV
0.1	0.492868	0.5000	−1.426458			
0.2	0.987501	1.0000	−1.249921			
0.3	1.482948	1.5000	−1.136717			
0.4	1.979041	2.0000	−1.047945			
0.5	2.475761	2.5000	−0.969506	0.092003	0.094535	−2.677884
0.6	2.973228	3.0000	−0.892385	0.191497	0.194535	−1.561637
0.7	3.471273	3.5000	−0.820732	0.291106	0.294535	−1.163964
0.8	3.969764	4.0000	−0.755906	0.390805	0.394535	−0.945447
0.9	4.468581	4.5000	−0.698196	0.490569	0.494535	−0.801985
1.0	4.967664	5.0000	−0.646725	0.590385	0.594535	−0.697940

Note. Percentage deviations are also tabulated.

torted grid network is omitted to reduce the CPU time. The temperature near the vapour/liquid interface is computed in a similar manner to that near the liquid/solid interface. Numerical results when $T_v = 1.5T_m$, $\omega = 2.0$, $r_f = 0.35$, and $\varepsilon_{min} = 0.01\,\%$ are shown in Table III and Figs. 9 and 10.

For accuracy assessment, the maximum percentage deviation for temperature (MPDT) is defined as

$$\text{MPDT} = \max\{((|\text{PDT}_{i,j}|), i = 0, N), j = 0, j_e\}, \quad (44)$$

where $\text{PDT}_{i,j}$ is the percentage deviation from the analytical temperature calculated at the nodal point (x_i, t_j) which is given by

$$\text{PDT}_{i,j} = 100 \times \frac{T_{Nu}(x_i, t_j) - T_{An}(x_i, t_j)}{T_{An}(x_i, t_j)}. \quad (45)$$

The maximum percentage deviation for time (MPDt) is given by

$$\text{MPDt} = \max\{(|\text{PDt}_j|), j = 0, j_e\}, \quad (46)$$

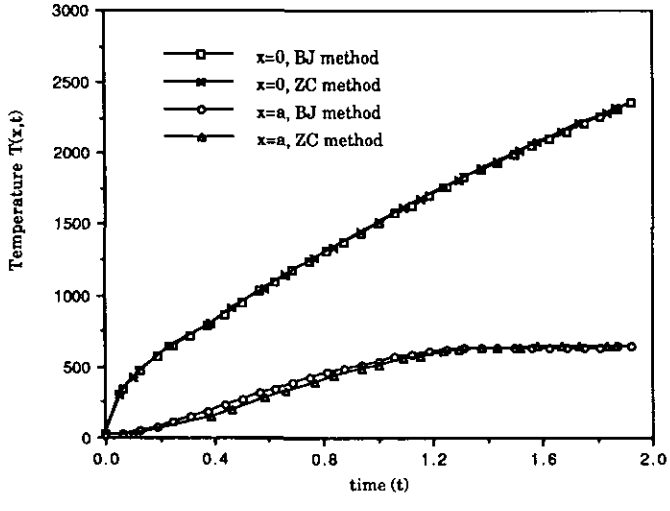

FIG. 7 (Problem 1b). Temperature versus time at different depths.

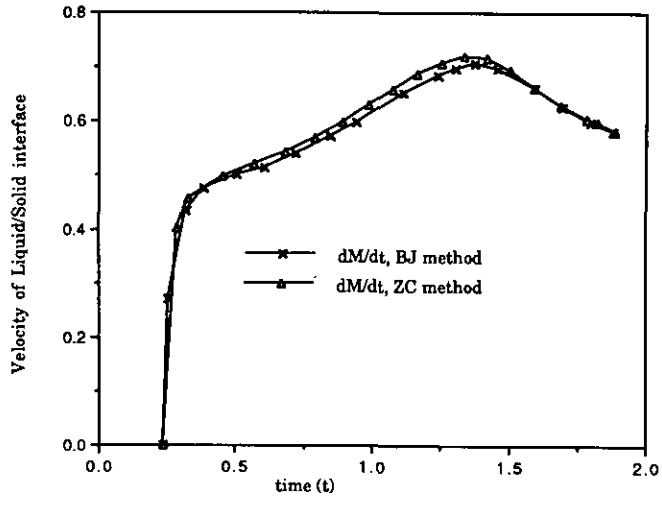

FIG. 8 (Problem 1b). Velocity of the moving boundary versus time.

where

$$\text{PDt}_j = 100 \times \frac{(t_j)_{Nu} - (t_j)_{An}}{(t_j)_{An}}. \quad (47)$$

The percentage deviation for vaporisation (PDV) interface position is given by

$$\text{PDV}_j = 100 \times \frac{(V_j)_{Nu} - (V_j)_{An}}{(V_j)_{An}}, \quad (48)$$

where the subscripts An and Nu refer to the value calculated analytically and numerically, respectively.

5. NUMERICAL RESULTS AND DISCUSSION

Numerical results show that for Problem 1a, which corresponds to a low conductivity material compared to

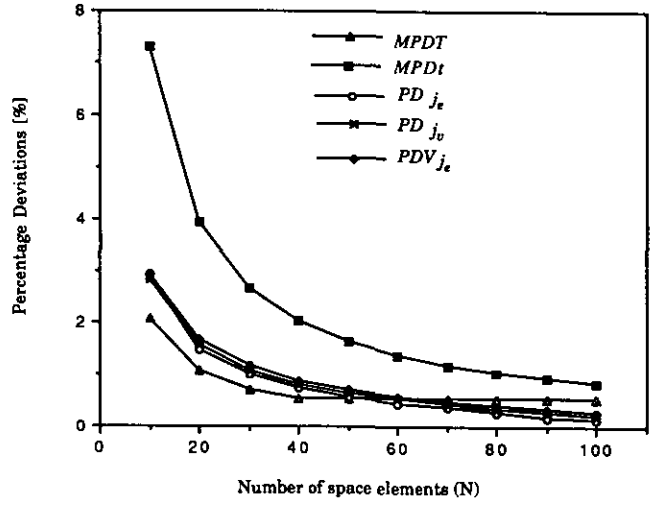

FIG. 9 (Problem 2). Percentage deviation for different variables of the solution versus the total number of space increments N ($\alpha = 0.1$).

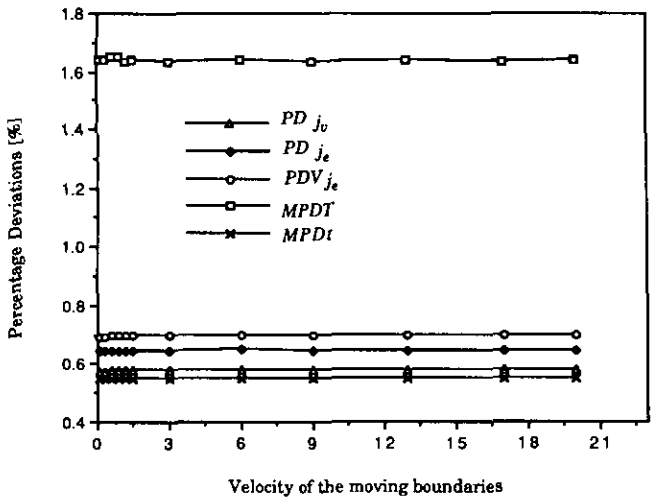

FIG. 10 (Problem 2). Variation of percentage deviations with velocities of the moving boundaries ($\Delta x = 0.02$).

that used in Problem 1b, the vaporisation occurs before the liquid/solid interface reaches the adiabatic boundary. On the contrary, in Problem 1b, the wall collapses before the appearance of a vapour/liquid interface and therefore the problem is one of melting only.

Table I, Figs. 3, 4, and 5 show that for Problem 1a, both the BJ and ZC solutions are in good agreement; a maximum relative error of only 2% occurs between the two solutions. For Problem 1a, the BJ method has a CPU time of 40 s, whereas the ZC solution takes only 9 s (non-vectorised program) on an IBM3090/150VF. The ZC scheme is more than four times faster than the BJ method. Using vectorisation, the speedup factor due to vectorisation varies from 2.5 to 3.5 for the BJ method, whereas it varies from 5 to 6 for the ZC method. This, however, is due to the fact that explicit methods are more suitable for vectorisation than implicit finite difference and finite element methods [11], where the unknown variables are determined with recurrent do-loops (i.e., do-loops that form a cycle of variable dependencies).

Figure 5 shows the velocity history of the two MBs for Problem 1a, where the L/S interface starts with zero velocity and reaches a maximum speed just after its appearance; its propagation speed then starts to decrease due the greater thermal-resistance of the liquid. When the V/L interface appears, the L/S interface slows sharply due the heat loss from vaporisation. The V/L interface accelerates sharply in the initial instance; then it continues to accelerate at a lower rate throughout the process. The L/S interface velocity reaches a minimum; then it starts to increase again. This is due to the fact that the heat flux entering the solid region decreases sharply when approaching the adiabatic extremity (i.e., there is less energy absorbed as the whole solid region approaches the melting temperature). The heat flux at the L/S interface decreases with a smaller gradient than the heat flux entering the solid region resulting in a greater proportion of the energy being available to melt the solid material; meanwhile, the V/L interface converges towards a constant acceleration due to the constant heat flux input. Before the total melting or the collapse of the wall, the L/S interface velocity starts to decrease due to the decreasing heat flux through the liquid and the absence of heat flux in the solid region.

As with Problem 1a there is good agreement between the two solutions for Problem 1b; this is shown in Table II, Figs. 6, 7, and 8. Unlike Problem 1a, the material used in Problem 1b is a good conductor of heat; therefore, the melting process is faster than that in Problem 1a. This can be seen from Fig. 8, where the velocity of the L/S interface is much higher than that predicted by Fig. 3; the wall collapses at $t = 1.8$ rather than $t = 9.2$ for Problem 1a. Unlike the behaviour of the L/S interface in Fig. 3, the melting interface for Problem 1b always accelerates due to the higher conductivity of the liquid, compared to that of the solid. At the end of the process the L/S interface has a similar behaviour to that of Problem 1a due to the adiabatic extremity.

Figure 9 shows that MPDT, MPDt, PDt_{j_e}, PDt_{j_e}, and PDV_{j_e} all decrease as N increases for Problem 2. In other words, the accuracy of the ZC method increases by increasing the total number of space elements which results in greater CPU time. It also can be seen that despite the singularities that appear with each moving boundary, the accuracy is very satisfactory. Maximum errors for the different variables of the solution are always generated at the appearance of a MB, these errors decrease with time as shown in Table II. Due to the incorporation of the VSIET, the accuracy of the present scheme is unaffected by the nature of the heat transfer problem; this can be seen from Fig. 10, where the percentage deviation for the different variables in the solution remain constant with the variation of moving boundary velocity. Therefore the method presented can be adapted to any heat transfer problem irrespective of its nature, and good accuracy can be achieved by tuning the parameters r_f, Δx, and $\varepsilon_{\min}$.

6. CONCLUSION

Vectorisation is an essential tool to increase performance and reduce the CPU time of large scale computation; explicit methods, where the unknown variables are determined with no recurrence (i.e., a group of statements that form a cycle of variable dependencies), are more suitable for vectorisation. However, if computations are to be performed for extended times, explicit methods do have instability constraints which make higher demands on computer memory requirements due to the large amount of data that must be stored. The significance of the method presented is that it combines the advantages of variable time step methods and explicit procedures whilst excluding their

disadvantages. The variable time-step approach requires less memory and storage requirements than a fixed grid network; this results in highly efficient use of the computational platform. The virtual sub-interval elimination technique ensures the stability of the scheme irrespective of the mesh size without increasing the array size; it also permits a high degree of vectorisation of the scheme.

APPENDIX: COMPUTATION OF TEMPERATURES AT THE FIRST TIME STEP

The dummy point temperature approach which is generally used to convert a heat flux to a fictitious temperature outside the domain is not a sufficiently accurate approach if the time step is relatively large at the beginning of the computation, where the solid is at constant temperature throughout. Therefore, in order to avoid instability of the scheme and, also, the need for extremely small increments, it is necessary to approximate the temperature at the first time step analytically. Since the temperature at $x=a$ remains unchanged during the time $0 \leqslant t \leqslant \Delta t_0$, the integral transform technique [12] was used to solve Eqs. (1) and (2) for a semi-infinite slab subjected to constant heat flux F_c at $x=0$, yielding the following solution for the temperature distribution:

$$T_s(x, t) = \frac{2F_c}{K_s}(\alpha_s t)^{1/2}\,\mathrm{ierfc}\left(\frac{x}{2(\alpha_s t)^{1/2}}\right) + T_0, \qquad 0 \leqslant t \leqslant \Delta t_0. \tag{49}$$

The heat flux during the time $0 \leqslant t \leqslant \Delta t_0$ is approximated by the average of $F(0)$ and $F(\Delta t_0)$, hence the temperature distribution at the time $t_1 = \Delta t_0$ is given by

$$T_{i,1} = \frac{F(0)+F(\Delta t_0)}{K_s}(\alpha_s \Delta t_0)^{1/2}\,\mathrm{ierfc}\left(\frac{i\,\Delta x}{2(\alpha_s \Delta t_0)^{1/2}}\right) + T_0, \qquad 0 \leqslant i \leqslant N, \tag{50}$$

where

$$\mathrm{ierfc}(x) = \frac{\exp(-x^2)}{\pi^{1/2}} - x\,\mathrm{erfc}(x), \tag{51}$$

$$\mathrm{erfc}(x) = 1 - \mathrm{erf}(x), \tag{52}$$

and

$$\mathrm{erf}(x) = \frac{2}{\pi^{1/2}}\int_0^x \exp(-y^2)\,dy. \tag{53}$$

Combination of (51) and (52) gives

$$\mathrm{ierfc}(x) = \frac{\exp(-x^2)}{\pi^{1/2}} - x(1-\mathrm{erf}(x)). \tag{54}$$

In order to reduce the computational time to the minimum possible, $\mathrm{erf}(x)$ is approximated within an error of $|\varepsilon(x)| \leqslant 1.5 \times 10^{-7}$ by [13],

$$\mathrm{erf}(x) = 1 - \exp(-x^2)\left[\sum_{i=1}^{5} a_i \left(\frac{1}{1+bx}\right)^i\right] + \varepsilon(x), \tag{55}$$

where

$$b = 0.3275911, \quad a_1 = 0.254829592, \quad a_2 = -0.284496736, \quad a_3 = 1.421413741, \quad a_4 = -1.453152027, \quad a_5 = 1.061405429. \tag{56}$$

ACKNOWLEDGMENTS

The financial assistance received by M. Zerroukat from the Algerian government is gratefully acknowledged. The authors would like to thank Dr. N. R. L. Maccallum and Dr. P. J. Larcombe for their valuable discussions.

REFERENCES

1. J. Stefan, *Sb. Akad. Wiss. Wien.* **98**, 965 (1889).
2. J. Crank, *Free and Moving Boundary Problems* (Clarendon Press, Oxford, 1984).
3. R. Bonnerot and P. Jamet, *J. Comput. Phys.* **41**, 357 (1981).
4. R. Bonnerot and P. Jamet, *J. Comput. Phys.* **32**, 145 (1979).
5. M. Zerroukat and C. R. Chatwin, *Int. J. Numer. Methods Eng.* **35**, 153 (1992).
6. W. L. Heitz and J. W. Westwater, *Int. J. Heat Mass Transfer* **13**, 1371 (1970).
7. S. C. Hsu, S. Chakravorty, and R. Mehrabian, *Metall. Trans. B* **9**, 221 (1978).
8. M. C. Bhattacharya, *Commun. Appl. Numer. Methods* **6**, 173 (1990).
9. M. C. Bhattacharya, An explicit conditionally stable finite difference equation for heat conduction problems, *Int. J. Numer. Methods Eng.* **21**, 239 (1985).
10. R. S. Gupta and D. Kumar, *Int. J. Heat Transfer* **24**, 251 (1981).
11. M. Zerroukat, Technical Report TR/GLU/MZ920830, Dept. Mech. Eng., University of Glasgow, 1992 (unpublished).
12. M. N. Ozisk, *Boundary Value Problems of Heat Conduction* (Int. Textbook, Scranton, PA, 1968).
13. M. Abramowitz and I. A. Stegun, *Handbook of Mathematical Functions* (Dover, New York, 1965).